Clim Dyn (2016) 46:2909–2921
DOI 10.1007/s00382-015-2740-9

Trend in frequency of extreme precipitation events over Ontario from ensembles of multiple GCMs

Ziwang Deng[1] · Xin Qiu[2] · Jinliang Liu[3] · Neal Madras[1] · Xiaogang Wang[1] · Huaiping Zhu[1]

Received: 16 January 2015 / Accepted: 29 June 2015 / Published online: 10 July 2015

Abstract As one of the most important extreme weather event types, extreme precipitation events have significant impacts on human and natural environment. This study assesses the projected long term trends in frequency of occurrence of extreme precipitation events represented by heavy precipitation days, very heavy precipitation days, very wet days and extreme wet days over Ontario, based on results of 21 CMIP3 GCM runs. To achieve this goal, first, all model data are linearly interpolated onto 682 grid points (0.45° × 0.45°) in Ontario; Next, biases in model daily precipitation amount are corrected with a local intensity scaling method to make the total wet days and total wet day precipitation from each of the GCMs are consistent with that from the climate forecast system reanalysis data, and then the four indices are estimated for each of the 21 GCM runs for 1968–2000, 2046–2065 and 2081–2100. After that, with the assumption that the rate parameter of the Poisson process for the occurrence of extreme precipitation events may vary with time as climate changes, the Poisson regression model which expresses the log rate as a linear function of time is used to detect the trend in frequency of extreme events in the GCMs simulations; Finally, the trends and their uncertainty are estimated. The result shows that in the twenty-first century annual heavy precipitation days, very heavy precipitation days and very wet days and extreme wet days are likely to significantly increase over major parts of Ontario and particularly heavy precipitation days, very wet days are very likely to significantly increase in some sub-regions in eastern Ontario. However, trends of seasonal indices are not significant.

Keywords Ontario · Extreme precipitation events · Index · Trend · Projection · Poisson regression

1 Introduction

Ontario, the most populated and the second largest province of Canada, extends approximately from 42°N to 57°N latitude and from 75°W to 95°W longitude. Its vulnerability to climate change is demonstrated by the impacts of recent severe weather events that caused natural disasters (Chiotti and Lavender 2008), for example the tornado in 2011 and ice storm in 2013. Thus, it becomes increasingly important for the provincial and local governments and the public to be aware of both current and future changes in extreme events as climate is likely to continue to change in the decades to come.

Previous studies show that as global climate change continues, total annual precipitation and the number of days with measurable precipitation have generally increased over Canada (Zhang et al. 2011). The trend toward increasing precipitation has been accompanied by increases in extreme daily precipitation amounts during the growing season (Qian et al. 2010). These increases can be attributed to climate change (Karl and Knight 1998); Adamowski and Bougadis (2003) examined precipitation intensities for various intervals and found significant trends in 5 and 10 min rainfall intensities; Mladjic et al. (2011) analysed the Canadian regional climate model (CRCM) projected changes

✉ Huaiping Zhu
huaiping@yorku.ca

[1] Lamps, Department of Mathematics and Statistics, York University, Toronto, ON M3J 1P3, Canada

[2] NOVUS Environmental, Guelph, ON N1G 4T2, Canada

[3] Department of Earth and Space Science and Engineering, York University, Toronto, ON M3J 1P3, Canada

in precipitation extremes, with the results showing an increase in 1-day precipitation extremes with a magnitude of 5–20 mm for 100-year return period. Many methods have been developed for detecting trends in climate data. For example, the least squares linear regression and Kendall's rank correlation have been widely used in detecting averaged climate variables (Kendall 1975; Zhang et al. 2000; Wang and Swail 2001; Vincent and Mekis 2006; Keim and Cruise 1998; Szeto 2008). For analyzing extreme events, a classic parametric method is the general extreme value (GEV) theory. The most common approach for applying this theory in climate extreme value analysis is to estimate the extreme quantiles using a GEV distribution based on three parameters: location, scale, and shape. However, this theory assumes that time series are stationary; for a changing climate, this assumption is clearly invalid (Wigley 1988), and thus an adjustment technique would need to be developed because the nature of climate change is considered non-stationary. If only analyzing whether there is a trend in the frequency of occurrence of an extreme event, not its severity, then the statistical technique of Poisson regression can be used (Katz 2010). The Poisson regression model is also known as the Generalized Linear Model (GLM) with Poisson error structure. Katz (2002) and Solow and Moore (2000) successfully used this method to fit trends in the frequency of historical North Atlantic hurricanes. The indices we will study in this paper are the counts of extreme events. As a widely used method for estimating the parameters in count or frequency model, the Poisson regression is a suitable method for investigating the trends in the count indices from ensembles of GCM output data for the future.

With the focus on the long term trend of heavy precipitation days (R10mm), very heavy precipitation days (R20mm), very wet days (R95p) and extreme wet days (R99p) across Ontario in the twenty-first century from ensembles of GCMs, the variations of severity of extremes or the total amounts of precipitation are not discussed in this paper. This study will provide useful findings about the relationship between changes in extreme conditions and other aspects of the distribution of daily precipitation; some statistical analysis will also be carried out on precipitation amounts such as wet-days, simple daily intensity index (SDII) and maximum one-day precipitation (Rx1D). The structure of the paper is as follows: Data is introduced in Sect. 2. Methods follow in Sect. 3. Trends simulated by different models are described in Sect. 4. Section 5 will summarize the conclusions of this study.

2 Data

Two types of data were used in this study: future projections and historical observations.

2.1 Model data: future projections

The simulations of most of the Coupled Model Intercomparison Project phase 5 (CMIP5) models were not available when we started this study. Therefore, future climate projections are the outputs from the ensemble of 21 GCM runs from the Coupled Model Intercomparison Project Phase 3 (CMIP3: Meehl et al. 2007) data archive at the Program for Climate Model Diagnosis and Intercomparison (PCMDI). The GCM results cover 3 time periods, 1968–2000, 2046–2065 and 2081–2100. The greenhouse gases emission scenario for the future climate is based on the Special Report on Emissions Scenarios A2 emission storyline (SRESA2) and the 20C3M scenario which was run with greenhouse gases increasing as observed through the twentieth century (IPCC 2000). Detailed descriptions of these models are presented in Table 1.

Currently, CMIP5 simulations are available. The CMIP5 builds on the CMIP3 in several ways, including a larger number of modeling centers and models, the use of generally moderately higher resolution models, and the inclusion of complex and complete representation of Earth system processes (Sheffield et al. 2014). However, the multi-model ensemble mean performance has not improved substantially in CMIP5 relative to CMIP3 for climatological variables, except for a slight improvement for near surface air temperature over land (Sheffield et al. 2014). A comparison study shows that there is more similarity than difference between CMIP3 and CMIP5 ensembles in their simulated seasonal cycle of precipitation in semiarid regions. The shift from

Table 1 List of the CMIP3 models used for analysis in this paper

Model name	Country	Run	Spatial resolution (lon × lat)
CCCMA-GCM3.1(T47)	Canada	1	3.75° × 3.75°
CCCMA-GCM3.1(T63)		1	2.81° × 2.81°
CNRM-CM 3	France	1	2.81° × 2.81°
CSIRO-Mk3.0	Australia	1	1.88° × 1.88°
CSIRO-Mk-3.5		1	1.88° × 1.88°
GFDL-CM2.0	USA	1	2.50° × 2.00°
GFDL-CM2.1		2	2.50° × 2.00°
GISS-AOM	USA	1	4.00° × 3.00°
GISS-EH		3	5.00° × 3.91°
GISS-ER		1	5.00° × 3.91°
IAP-FGOALS-g1.0	China	1	2.81° × 3.00°
INM-CM3.0	Russia	1	5.00° × 4.00°
MIROC3.2(medres)	Japan	1	2.81° × 2.81°
MPI-ECHAM5	Germany	1	1.88° × 1.88°
MRI-CGCM2.3.2	Japan		2.81° × 2.81°
NCAR-CCSM3	USA	3	1.41° × 1.41°
NCAR-PCM		1	2.81° × 2.81°

CMIP3 to CMIP5 is typically much less than one standard deviation of either ensemble. CMIP3 and CMIP5 are also consistent in the simulated precipitation trend (Baker and Huang 2014). The CMIP5 RCP8.5 (representative concentration pathway 8.5) is close to the CMIP3 SRESA2 used in this study (van Vuuren et al. 2011). Therefore, the trend analyses from CMIP3 ensemble are still useful.

2.2 Reanalysis data: historical observations

Using homogeneous historical observation data set for model calibration and validation is the best choice in statistical model construction. However, weather stations are distributed unevenly in Ontario. Sparse in vast central and northern areas, the majority of stations are located in southern Ontario and most of the weather stations have a record length less than 20 years (Adamowski and Bougadis 2003). The best alternative in the face of incomplete and inconsistent observed data sets is using reanalysis products, because reanalysis products represent dynamically-consistent estimates of the state of climate system using the best blend of past, current, and perhaps future observations. There are some high resolution daily reanalysis data sets that cover Ontario, for example the new generation of ECMWF reanalysis climate data (ERA-interim, Dee et al. 2014), NCEP North America Regional Reanalysis (NARR 2013) and the NCEP climate forecast system reanalysis (CFSR, Saha et al. 2010, 2013). An evaluation of these reanalysis datasets in representing frequencies of extreme precipitation events is necessary before using them for bias correction. A simple comparison of the days with daily precipitation >10 mm and days with daily precipitation >25 mm, derived from the reanalysis datasets and from observations for the period 1981–2010 over 30 stations in Ontario (http://climate.weather.gc.ca/climate_normals/index_e.html), shows that among the three datasets, the CFSR dataset better estimates frequency of the heavy precipitation events in Ontario (Deng et al. 2015). Therefore, in this study we use the climate forecast system reanalysis (CFSR) data as observations for model calibration and validation.

The CFSR is a third generation reanalysis product, with higher temporal (6-h) and spatial resolution (0.313-deg x ~ 0.312-deg) completed recently at the National Centers for Environmental Prediction (NCEP). It has assimilated observations from many data sources and has improved the simulation of time–mean precipitation distribution over various regions compared to the previous generations of reanalyses (Saha et al. 2010; Wang et al. 2011; Saha et al. 2013). Despite CFSR did not directly assimilate precipitation observations, it assimilated many hydrological quantities from a parallel land surface model forced by the NOAA's Climate Prediction Center (CPC) pentad merged analysis of precipitation and the CPC unified daily gauge analysis. (Wang et al. 2011). Although the improved data used in CFSR are not sufficient to eliminate the bias, the magnitude of the bias in CFSR is reduced compared to the previous generations of NCEP reanalysis (Higgins et al. 2010). The daily precipitation of CFSR has been widely used for verification of deterministic precipitation forecasts and validation of downscaling methods (Stefanova et al. 2011; Moore et al. 2015; Kishore et al. 2015).

3 Methods

3.1 Bias correction

Ontario's climate is affected by three major climate impact factors: cold and dry polar air from the north which is the dominant factor during the winter months; Pacific polar air passing over the western prairies; and warm, moist, subtropical air from the Atlantic Ocean and the Gulf of Mexico (Baldwin et al. 2011). The effect of these major air flows on precipitation depends on latitude, proximity to major water bodies (the Great Lakes, Hudson Bay and James Bay), and, to a limited extent, terrain relief (flat plains, low-uplands, escarpments or cuestas). The limited representation of regional orography and poor representation of mesoscale processes in GCMs makes it impossible to accurately simulate some of the precipitation events, especially the extreme precipitation events; consequently, climate downscaling and bias correction are necessary before calculating the precipitation indices in a refined spatial resolution.

The CMIP3 models can simulate heavy precipitation events reasonably well over northern and eastern Canada and capture the seasonal cycle of heavy precipitation over a majority of North America, but tends overestimate the intensity of light precipitation events over much of North America (Deangelis et al. 2013). However, since this study focuses on extreme precipitation events, we only deal with the wet day precipitation and the light precipitation events are of less concern. GCM precipitation, in some sense, integrates all relevant large-scale predictors and therefore is a good predictor for statistical downscaling (Widmann et al. 2003). Deviations between the large-scale GCM precipitation and regional precipitation are due to biases from systematic errors in GCMs and their incapability to resolve mesoscale dynamics such as deep convection or realistic surface orography. On the contrary, the higher resolution CFSR data can perform better to reflect the impacts of real surface orography or mesoscale processes on precipitation. A relationship between GCM and CFSR data in the overlaid historical period (1979–2000) could be used to reduce the error in GCM projections. To simplify the computations in our analysis, the outputs from GCMs and CFSR data completed by the National Centers for Environmental

Prediction (NCEP) for the reference period (1981–2000) are interpolated onto a common 0.45° × 0.45° grid using an inverse distance-weighting method (Li et al. 2012; Shen et al. 2001). There are total of 682 grid points in Ontario. Then, a local intensity scaling (LOCI, Schmidli et al. 2006) method is used to reduce errors in the interpolated GCM modelled precipitation.

Previous comparisons of downscaling methods show the performance of the LOCI is in most cases comparable to the best downscaling models (Schmith 2007; Gao et al. 2014). LOCI multiplies the model precipitation with the ratio of the observed to modelled intensity of wet day precipitation. Researchers (e.g., Waggoner 1989; Watterson 2005) have demonstrated that the most preferred distribution to fit wet-day rainfall amounts is the 2-parameter Gamma distribution function. Our experiments showed the wet-day precipitation from the CFSR data over Ontario fits the 2-parameter Gamma distribution very well. Therefore, in this study, the 2-parameter Gamma distribution is used to fit wet-day precipitation. The intensity of precipitation is represented by the product of the 2 parameters. The goal of precipitation bias correction is to make the model data and reanalysis data have the same total wet days for the common historical period 1979–2000 and same estimated expectation ($E = \alpha \times \beta$), where α and β are respectively the shape and scale parameters of the Gamma distribution. This method adjusts the precipitation series at each of the 682 grid points in Ontario by removing the bias in wet-day frequency and intensity. It is capable of reducing large biases in the precipitation frequency distribution, even for high quantiles (Schmidli et al. 2006). So, LOCI is a robust method to directly correct GCM or RCM outputs for local observations (Gao et al. 2014). The key of using LOCI is to estimate the threshold of wet-day precipitation R_c and the intensity adjustment coefficient r. To achieve these goals, firstly, we find the threshold of wet days at each grid point for each ensemble member by the following formula based on the historical 22 years data (1979–2000):

$$\boldsymbol{R_c}(\text{condition: sum}(\text{R}\boldsymbol{R_c}\text{mm}_\text{m}) = \text{sum}(\text{R}\mathbf{1}\text{mm}_\text{o})) \quad (1)$$

where R_c is the threshold value of model data which guarantee the total wet days (daily precipitation $\geq R_c$) of model data exactly equals the total wet days (daily precipitation ≥ 1 mm) of CFSR data for the reference period. Using this method, we can find the R_c for each GCM run at a grid point.

After determining the threshold of wet-day precipitation, the next step is to adjust the intensity of wet-day precipitation to make the estimated expectation (E_m) of GCM data at a grid point equal that of the reanalysis data (E_o), i.e. ($E_m = E_o$). Two steps are needed to get the adjustment coefficient ($r = r_1 r_2$). Firstly, we use the following formula to adjust the model wet day precipitation data:

$$y^{(1)} = (y - \boldsymbol{R}_c) \times r_1 + 1.0 \quad (2)$$

where $y^{(1)}$ and y are the model value after and before correction respectively, $r_1 = \frac{\mathbf{E}_o}{\mathbf{E}_m^{(0)}}$, $E_m^{(0)} = \alpha_m^{(0)} \times \beta_m^{(0)}$ and $E_o = \alpha_o \times \beta_o$ is estimated expectation of wet day precipitation of the model run and the CFSR for the overlap period (1979–2000). $\alpha_m^{(0)}$ and $\beta_m^{(0)}$ are shape and scale parameter of model data respectively, α_o and β_o are the shape and scale parameters of CFSR data respectively, and the value 1.0 mm is standard threshold value of observed wet day. After using Eq. (2), the threshold of wet day of the model data ($\boldsymbol{R_c}$) is replaced with 1.0 mm. Subsequently, the shape and scale parameters of the adjusted model data change from $\alpha_m^{(0)}$ and $\beta_m^{(0)}$ to $\alpha_m^{(1)}$ and $\beta_m^{(1)}$. Therefore the result from Eq. (2) should be further corrected using the following equation

$$y^{(2)} = \left(y^{(1)} - 1.0\right) \times r_2 + 1.0 \quad (3)$$

where $r_2 = \frac{\mathbf{E}_o}{\mathbf{E}_m^{(1)}}$, and $\mathbf{E}_m^{(1)} = \alpha_m^{(1)} \times \beta_m^{(1)}$ is the estimated expectation of model wet day precipitation from Eq. (2). Finally, the estimated expectation of model data from Eq. (3), $\mathbf{E}_m^{(2)} = \alpha_m^{(2)} \times \beta_m^{(2)}$, is exactly equals to E_o. With this method, we can get R_c and coefficient $r = r_1 r_2$ at each grid point for each ensemble member. Then they are used to correct the wet-day daily precipitation amount for the 3 periods. As an example, Fig. 1 shows the effect of bias correction on wet day precipitation from CGCM3.1 at 2 grid points close to Toronto (79.4 W, 43.67 N) and Pickle Lake (90.22 W, 51.45 N). It is clear that the LOCI method is capable of correcting the bias in the wet day daily precipitation amount.

3.2 Indices calculation

This study focus on the trend of 2 threshold indices, heavy precipitation days (R10mm) and very heavy precipitation days (R20mm), and 2 percentile indices: very wet days (R95p) and extreme wet days (R99p). The calculations of these indices follow the guidelines proposed by Albert et al. (2009). Here, the symbols R95p and R99p represent count of very wet days and extreme wet days rather than total precipitation amount of very wet days and extreme wet days used in Albert et al. (2009). After bias correction, it is straightforward to estimate the seasonal and annual values of the indices R10mm and R20mm for a specific year by directly counting the days with daily precipitation amount greater than the given thresholds of 10 and 20 mm. The R95p and R99p represent days with significant anomalies relative to the local climate defined by the sample of all wet days in the base period. The thresholds for the R95p and R99p are estimated based on the 22 years CFSR wet day daily precipitation data for each of the 682 grid points.

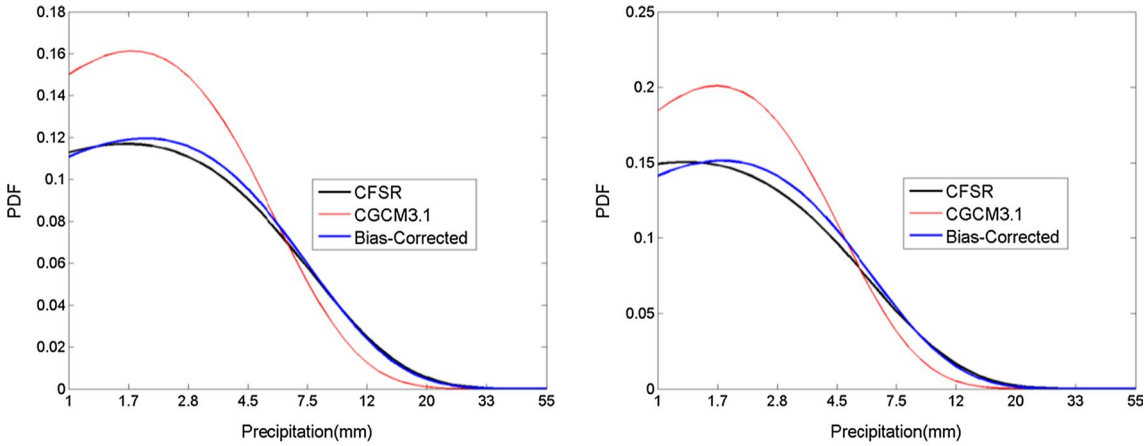

Fig. 1 The fitted probabilistic density functions of wet-day precipitation from CFSR (*black*), interpolated CGCM3.1 (*red*) and the bias-corrected CGCM3.1 (*blue*) data at Toronto (*left* 79.4 W, 43.67 N) and Pickle Lake (*right* 90.22 W, 51.45 N)

Table 2 Definition of indices (Albert et al. 2009)

Index	Name	Definition	Description
R1mm	Wet days	Count of days where RR > 1 mm	Let RRij be the daily precipitation amount on day i in period j. Count the number of days where RRij ≥ 1 mm
SDII	Simple daily intensity index	Mean precipitation amount on a wet day	Let RRij be the daily precipitation amount on wet day w (RR ≥ 1 mm) in period j. If W represents the number of wet days in j then the simple precipitation intensity index SDIIj = sum (RRwj)/W
RX1D	Maximum one-day precipitation	Highest precipitation amount in one-day period	highest precipitation amount in one-day period
R10mm	Heavy precipitation days	Count of days where RR > 10 mm	Let RRij be the daily precipitation amount on day i in period j. Count the number of days where RRij ≥ 10 mm
R20mm	Very heavy precipitation days	Count of days where RR > 20 mm	Let RRij be the daily precipitation amount on day i in period j. Count the number of days where RRij ≥ 20 mm
R95p[a]	Very wet days	Count of days where RR > 95th percentile	Let RRwj be the daily precipitation amount on a wet day w (RR ≥ 1 mm) in period j and let RRwn95 be the 95th percentile of precipitation on wet days in the base period n (1981–2010). Count the number of days where RRwj > RRwn95
R99p[a]	Extreme wet days	Count of days where RR > 99th percentile	Let RRwj be the daily precipitation amount on a wet day w (RR ≥ 1 mm) in period j and let RRwn99 be the 99th percentile of precipitation on wet days in the base period n (1981–2010). Count the number of days where RRwj > RRwn99

[a] R95p and R99p count of very wet and extreme wet days which are different from Albert et al. (2009)

Using the number of days exceeding percentile thresholds is more evenly distributed in space and is meaningful in every region (Albert et al. 2009). As mentioned in the introduction, 3 general precipitation amounts (R1mm, SDII and Rx1D) are also estimated. The definitions of these indices are presented in Table 2. These indices are calculated from CFSR data for period 1979–2009 and from downscaled GCM ensemble data for periods 1968–2000, 2046–2065 and 2081–2100.

3.3 Trend detection

Trend detection methods vary with the variables according to their properties. In this study, we will use the linear

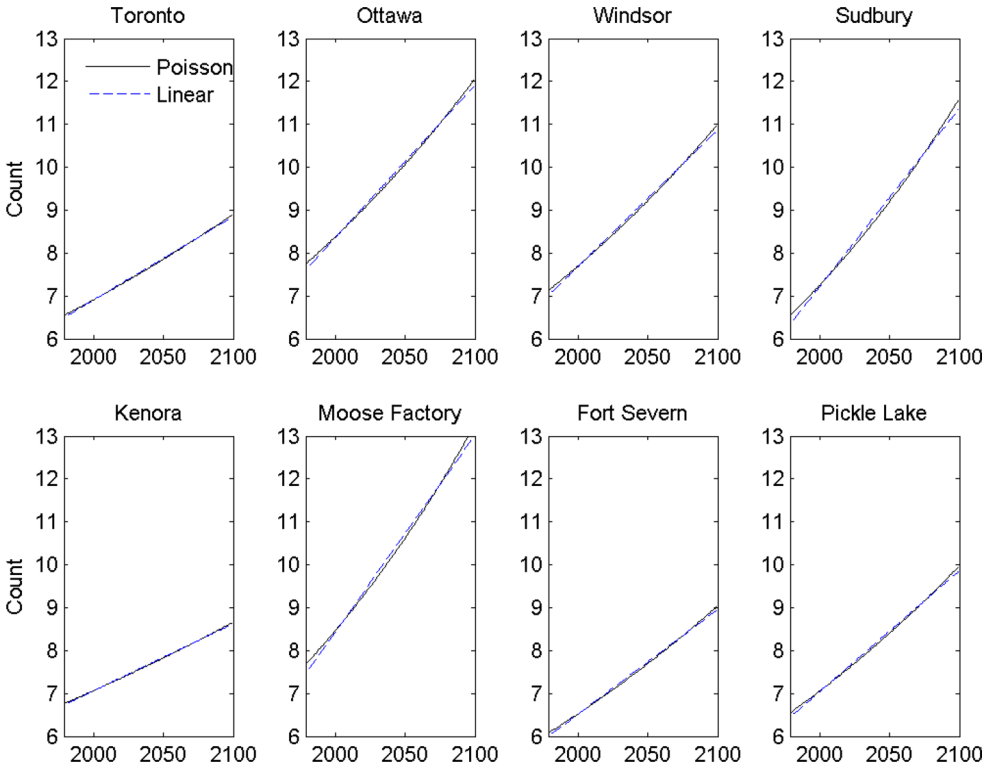

Fig. 2 Comparison of trend lines estimated with the Poisson regression (*solid black line*) and the linear regression (*dashed blue line*) for very wet days (R95p) based on the CCSM4 model output for the period 1979–2100

regression method to detect the trend in spatial mean indices and the Poisson regression to detect the trend in the indices at each grid point. Because trends in normally distributed continuous variables are usually detected with the linear regression method and the spatial mean of the indices are assumed to follow the normal distribution according to the central limit theorem, therefore their trends are detected using the following formula:

$$K = K_0 + at \tag{4}$$

where K is the averaged index, K_0 is the intercept and $\boldsymbol{\alpha}$ is the regression coefficient, t is time (in year). The *F* test is used to check significance of trends.

On the contrary, the change of the counting number could be considered as a counting process which is usually described by the Poisson distribution. Katz (2002) and Solow and Moore (2000) proposed to use the statistical technique of Poisson regression to examine the trend in these count data. Katz (2002) and Solow and Moore (2000) used this technique to fit trends in the frequency of hurricanes. As counting numbers, the trend of R10mm, R20mm, R95p and R99p at a grid points could also be estimated with the Poisson regression. The Poisson regression method assumes a linear trend in the logarithm of the rate parameter of the Poisson distribution following the method used in Katz (2002) and Solow and Moore (2000):

The Poisson distribution assumption is

$$\mathrm{P\{N = k\}} = \frac{\mathrm{e}^{-\lambda}\lambda^{\mathrm{k}}}{\mathrm{k!}}, \quad \lambda = \mathrm{E[N]} = \mathrm{Var[N]} \tag{5}$$

where N is the counting number, P{N = k} is the probability of k events occurring.

The non-stationary assumption is

$$\ln\left[\lambda(\mathrm{i})\right] = \alpha + \beta \mathrm{i}, \quad \mathrm{i} = 1, 2, \ldots, \mathrm{m}, \tag{6}$$

where $\lambda(i)$ denotes the rate (days) of climate events in the ith year, β is the slope parameter of the trend curve. It is estimated with maximum likelihood estimation (MLE). A positive (negative) β value denotes an increasing (decreasing) trend. For a grid point, if β passes the χ^2 test (at a 0.05 significance level), then we can say there is a significant increasing (decreasing) trend in the index at the grid point. We will perform this analysis to the index ensemble from downscaled GCMs. As examples, Fig. 2 shows the trend lines of R95p at the 8 grid points shown in Fig. 1 for the period 1979–2100 from CCSM3 model. For comparison, the trend lines generated with the simple linear regression method are also plotted in the figure. It is clear that the trend lines estimated with the two methods are very close at each of the locations. All of the trend coefficients estimated with Eqs. (4) and (6) pass the significant tests. Although we got similar results with these two methods, we will only show the results based on the Poisson regression method.

4 Results

4.1 Trends of spatial averaged indices in the last 3 decades

Before investigating the model simulation, it is necessary to examine the variations of the indices during the last 3 decades over whole province. At first, the spatial mean of an index is calculated by averaging the index values for each year over all 682 grid points. Then, trend analysis is performed to it using the formula (4). Finally, the *F* test is performed to check whether the trend is significant. Figure 3 shows the spatial mean values of seasonal and annual R1mm, R10mm and R20mm based on CFSR data for the past 31 years (1979–2009). MAM (March, April and May), JJA (June, July and August), SON (September, October and November), DJF (December, January and February) and ANN (January–December) represent time periods (i.e., spring, summer, autumn, winter and year) for estimating the indices. The *F* test results are indicated by different line types and colors. In Fig. 1, linear trends are observed in some indices. For example, the increasing trends in ANN R10mm, ANN R20mm, and JJA R20mm are significant at the 5 % level (solid thick line), and the increasing trends in JJA R1mm, JJA R10mm, SON R10mm and SON R20mm are significant at the 10 % significance level (dashed thick line). However, the trends in other indices cannot pass the significant test at either the 5 % or the 10 % level. These results reveal the fact that the heavy (R10mm) and very heavy precipitation days (R20mm) have significantly increased in Ontario during the last 3 decades, despite the annual total wet days (R1mm) kept stable. The increases mainly occurred in summer and autumn.

4.2 Change of spatial averaged indices in future

For the future periods 2046–2065 (period 2) and 2081–2100 (period 3), we calculated the spatial mean for each ensemble member. Then, based on this ensemble we generate the boxplots as shown in Fig. 4. The median (50th percentile), middle range (blue box, 25–75 %), low-estimate (10th percentile) and high-estimate (90th percentile) of the 5 count indices are plotted. For comparison, the mean values for the period 1980–2009 (period 1) are plotted as stars in Fig. 4. According to the calibrated language for describing quantified uncertainty, if the proportion of ensemble members that show increasing trend is ≤10 %, ≤33 %, ≤66 % or >90 %, we say the increase trend is very unlikely, unlikely, likely or very likely, respectively (Mastrandrea et al. 2010). Therefore, the 33th percentiles and 66th percentiles are also plotted in the figure as red '+' and blue '+' respectively. Comparing the medians for the 3 periods, it is observed that most of the indices will increase in the future. The exceptions are SON R1mm and

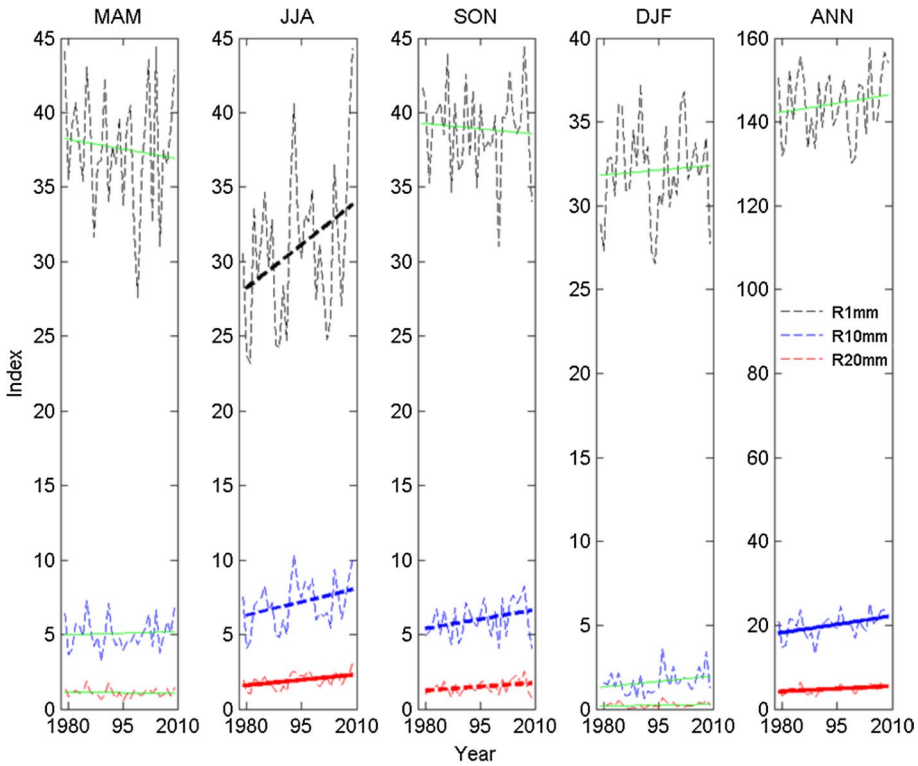

Fig. 3 Variations of spatial averaged seasonal and annual indices. The *dashed thin black*, *blue* and *red lines* represent inter-annual variations of wet days, heavy precipitation days and very heavy precipitation days from the CFSR data for the last 31 year respectively. The *solid* and *dashed thick straight lines* represent that the linear trends pass the *F* test at the 5 and 10 % significance levels respectively. The *green thin straight lines* indicate the linear trends pass neither 5 nor 10 % significance test

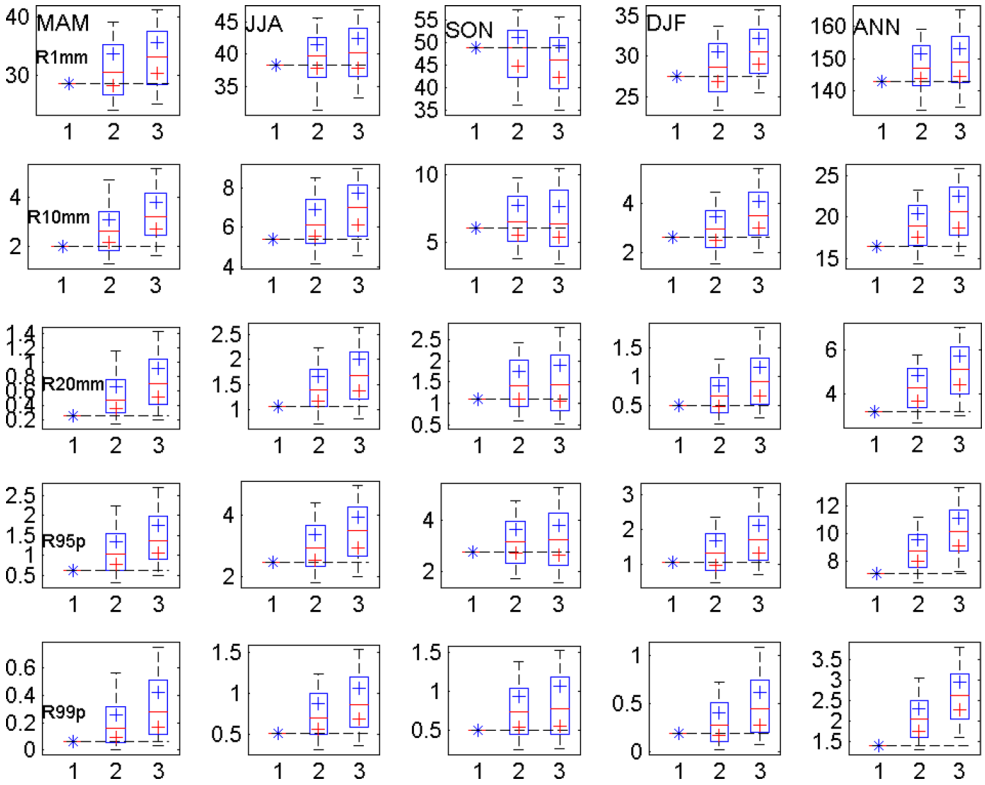

Fig. 4 Boxplot of spatial averaged seasonal and annual indices from the downscaled ensemble for period 2 (2046–2065) and period 3 (2081–2100). The *star* represent the 30-year mean value for period 1980–2009), the *red horizontal line* represent the median, the *box portion* represent the 25th percentile to 75th percentile, the *whiskers* represent the 10th percentile (lower-estimate) and the 90th percentile (high-estimate) and the *red* "+"s mark the positions of the 33rd percentile and the *blue* "+"s mark the positions of the 66th percentile

SON R10mm which may decrease in 2081–2100 relative to the period 2046–2065. The middle range and the 10–90 percentile range indicate that the uncertainty of the estimation is larger in the end of the century than in the middle of the century. It is evident that almost all 10th percentiles are smaller than current values implying the possibility of decrease of the indices in the future. The subplots of the annual indices show that all 33th percentiles are greater than the current values, therefore all of the indices are likely (>66 %: red crosses are above the horizontal dashed black lines) to increase in the future. However, only annual percentile indices R95p and R99p are very likely (>90 %) to increase for 2081–2100 relative current. It is evident that the four extreme indices are likely to increase in MAM, JJA and ANN for both of the two future periods and are likely to increase in DJF for 2081–2100 relative to current situation.

4.3 Frequency and intensity of precipitation

Before discussing extreme climate/weather events, we first examine the change of mean frequency and intensity of precipitation averaged over the three 20-year periods in Ontario. The indices R1mm and SDII are usually used to represent frequency and intensity of rain. The average values of these indices from CFSR data for 1981–2000 and from ensemble mean for 2046–2065 and 2081–2100 are plotted with geographic information system software ArcGIS 10.2.2 (http://resources.arcgis.com/en/home/). The results are shown in Fig. 5. Smaller values are displayed with warm colors and bigger values are displayed with cool colors. Comparing changes of the colors at each grid in the 3 subfigures in the top and middle rows, it is observed that the annual R1mm and SDII increase in the 2 future periods relative to the current period over most grid points in Ontario. While the mean situation changes, the extreme situation also changes with time. The 20-year mean of maximum one-day precipitation (Rx1D) is also shown in Fig. 5, the annual Rx1D will also increase at most grid points. We did not find any grid point that shows decrease for the 3 periods.

4.4 Frequency of extreme precipitation events

The ensemble mean of the 4 precipitation related extreme climate indices R10mm, R20mm, R95p and R99p for the 3 periods are shown in Fig. 6. It is evident that as wet-days and intensity of precipitation increase, the events of extreme precipitation will also increase. Thus, the heavy precipitation days (R10mm), very heavy precipitation days (R20mm), very wet days (R95p) and extreme wet days (R99p) will increase in the future (Fig. 6). Because heavy and very heavy precipitation events mainly happen in south part of Ontario, the increases in R10mm and R20mm are larger in southern Ontario. The increases of percentile indices R95p and R99p are more uniform in space.

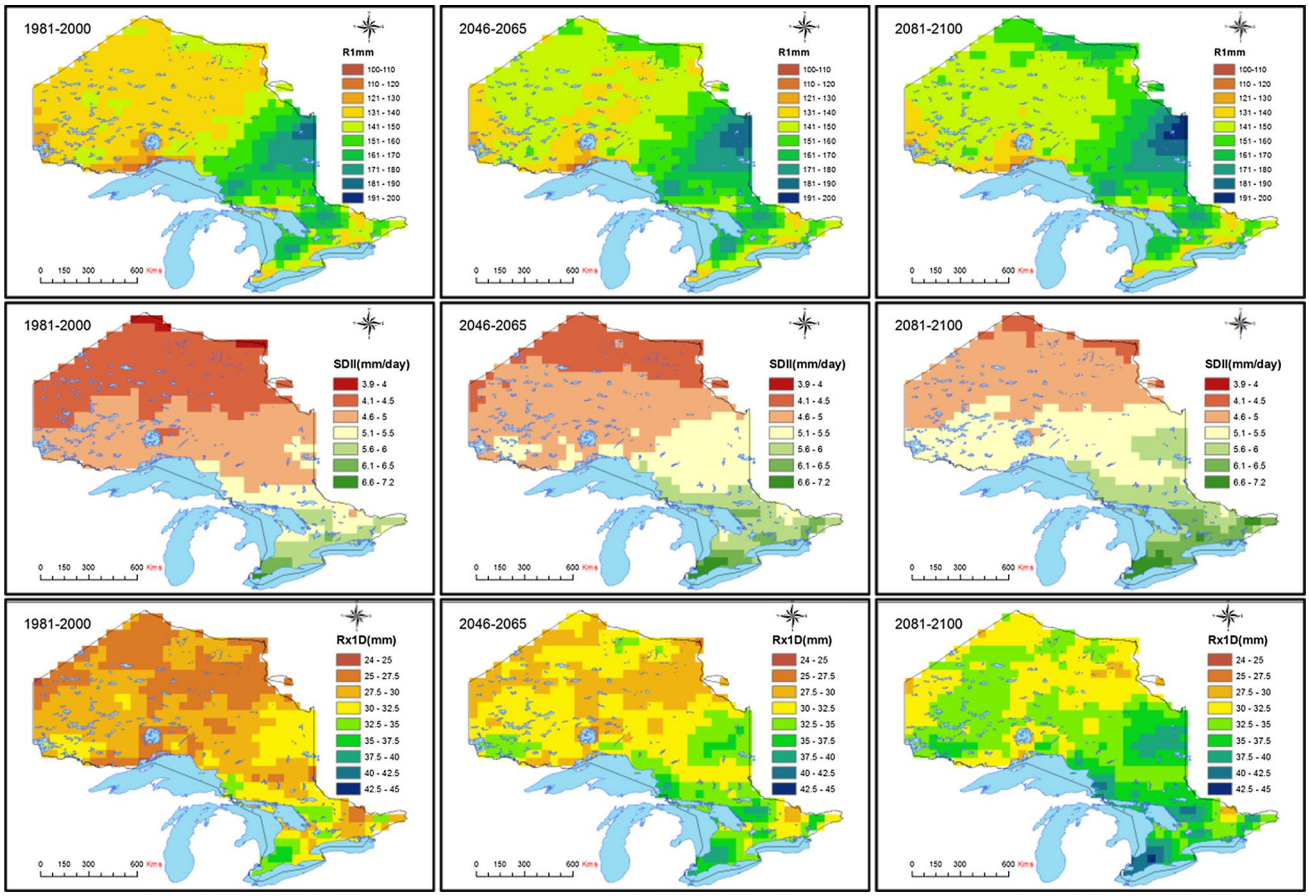

Fig. 5 Temporal average of ensemble mean of annual wet days (R1mm, unit: days), simple daily intensity index (SDII) and maximum one-day precipitation (Rx1D) for the 3 periods 1981–2000 (*left*), 2046–2065 (*middle*) and 2081–2100 (*right*)

4.5 Likelihood of significant trends

Combining data for the 3 periods and using Eq. (6), we can estimate the trend coefficient at each model grid for each index from an ensemble member. A positive (negative) coefficient indicates an increasing (decreasing) trend. The portion (in %) of the number of models which have positive (negative) coefficients out of the 21 models can quantify the uncertainty of the trend. The results show that over 90 % of the models present positive trend coefficients in all of the seasonal and annual indices over Ontario. However, the non-zero trend coefficient may be a result of various stochastic noises. Thus, the trend coefficients that cannot pass the significance test may be meaningless. Therefore, further analysis of the portion of coefficients that pass the significance test is necessary. The significance of the trend coefficient β of the parameter for each index at each grid from a model run can be tested by χ^2 significance test.

Based on the significance test of the trends from the 21 GCM runs for the 3 periods, the percentages of ensemble members with significant increasing trend coefficients for seasonal and annual indices can be estimated. Figure 7a, c show that annual heavy precipitation days (R10mm) and very wet days (R95p) are likely (>66 %) to significantly increase over almost all of the grid points in Ontario and are very likely (>90 %) to significantly increase in the northeastern Ontario. Figure 7b, d show that very heavy precipitation days (R20mm) and extreme wet days (R99p) are likely to significantly increase over a major area except for the northwestern region. At some grid points in the central area, R20mm are very likely to significantly increase. Further checking the portions of seasonal indices of increasing trend (not shown), it is evident that in almost all seasons the indices are likely to increase, however, at most grid points, more than half (>50 %) of the trend coefficients cannot pass the significance test. Only in some grid points, for example in the central area, the MAM R10mm and DJF R10mm are likely to significantly increase. Failure to pass the significance test is possibly due to the large inter-annual variance in the time series of the seasonal indices which may lead to type II error.

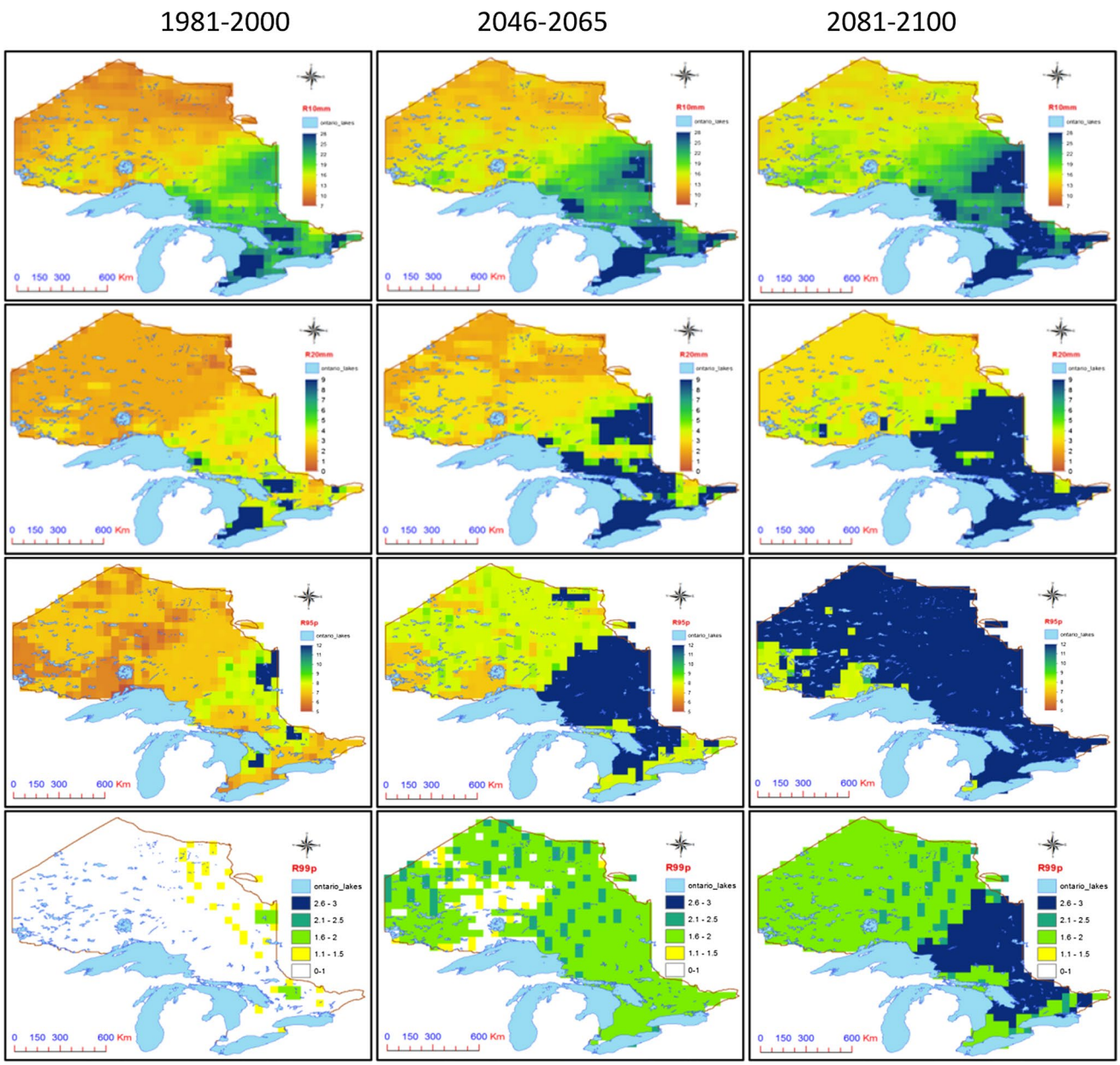

Fig. 6 Temporal average of ensemble mean of indices (in days) heavy precipitation days (R10mm: *top row*),very heavy precipitation days (R20mm: *second row*), very wet days (R95p, *third row*) and extreme wet days (*bottom row*) for the three 20-year periods 1981–2000 (*left*), 2046–2065 (*middle*) and 2081–2100 (*right*)

5 Summary and discussion

In this study, the long term trends in frequency of occurrence of extreme precipitation events represented by indices R10mm, R20mm, R95p and R99p, over Ontario, are investigated. The data examined are the results from an ensemble of CMIP3 GCMs. For simplicity, all model data are linearly interpolated onto a grid with resolution of 0.45° × 0.45°. As a reference data, the high resolution CFSR reanalysis precipitation data for 1979–2009 is used to correct the biases in wet day precipitation from models for current and future periods. Considering the effects of local geographic factors, the local intensity scaling (LOCI) method is used to adjust the wet day precipitation. The seasonal and annual extreme precipitation indices are estimated for the current and future periods. The trends of spatial averaged indices are fitted with the linear regression model and the trends of the indices at each model grid point are fitted with the Poisson regression model. The Poisson model assumes the underlying probability distributions

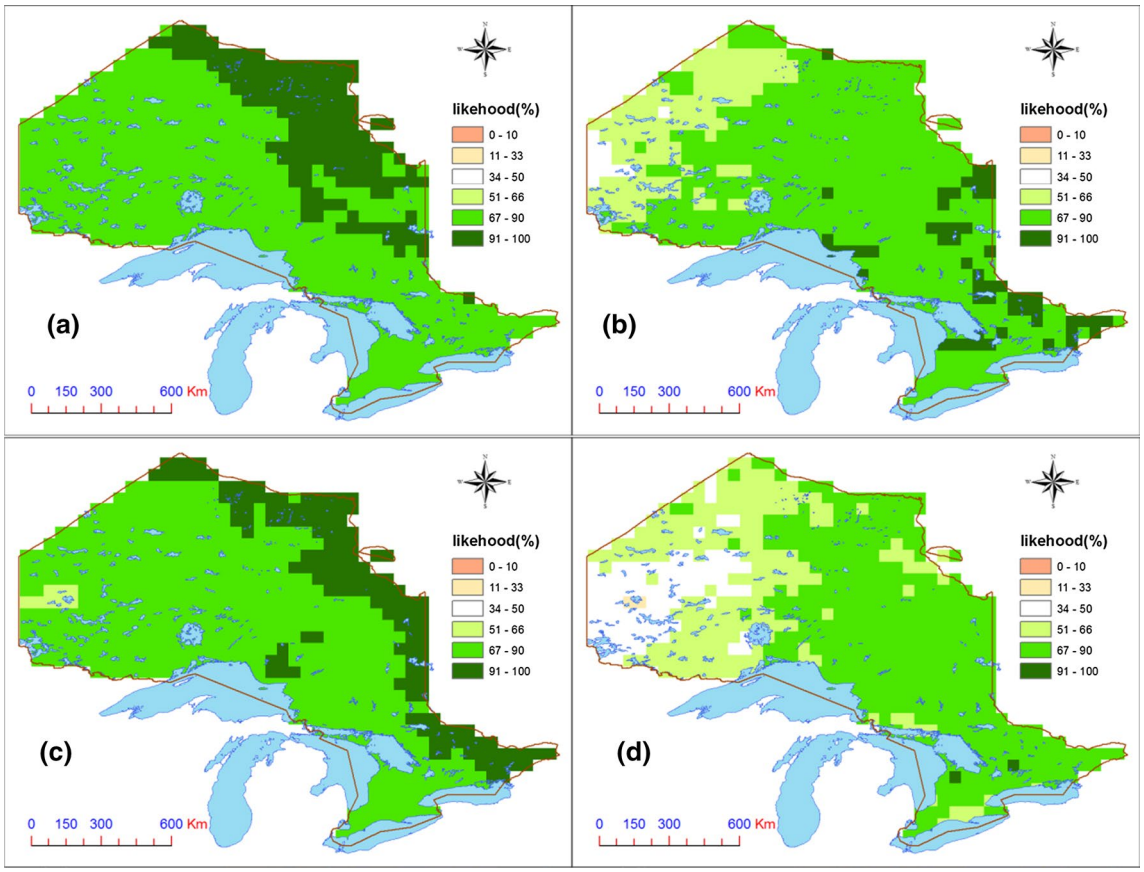

Fig. 7 Spatial distribution of percentages (in %) out of the models with significant increasing trend in the four annual indices. **a** R10mm, **b** R20mm, **c** R95p, **d** R99p

of these count indices slowly change as global climate changes. The uncertainties which are quantified with likelihood of significant trends in the indices at grid points are estimated based on the 21-member ensemble.

The result shows that the spatial mean of the indices significantly increased in the last 3 decades and are likely to continually increase in this century. Comparing the ensemble means for the 3 periods indicates the frequency and intensity of precipitation and maximum one-day precipitation will increase in the future. Spatially, the annual values of the 4 extreme precipitation indices are likely to significantly increase over major part over Ontario in twenty-first century. The annual R10mm and R95p are very likely to significantly increase at some points in the east area. The increasing trends are consistent with some recent studies from the low resolution GCMs under the RCP8.5 (Baker and Huang 2014; Kharin et al. 2013; Sillmann et al. 2013; Maloney et al. 2014). For example, the magnitude of the precipitation extremes over land increases appreciably with the multi-model median increasing by about 30 % in the RCP8.5 experiments by the year 2100 (Kharin et al. 2013). Over Ontario, heavy precipitation days (R10mm) increases by about 4–6 days and very wet day precipitation increase by about 40–70 % (Sillmann et al. 2013). Precipitation increases 0–0.25 mm/day in summer and 0.25–1 mm/day in winter for 2080s in RCP8.5 (Maloney et al. 2014).

Since strong warming in Ontario is a robust characteristic of future climate change projections, increases in extreme precipitation may follow the warming in temperature according to the Clausius–Clapeyron relationship that predicts an increase in moisture availability of about 6–7 % per °C. (Kharin et al. 2013). The changes in the structure of global and regional atmospheric circulation caused by the warmer climate may affect the frequency of extreme precipitation events as well (Thomas 2009). Some studies show the increase in frequency of precipitation events in cold season is associated with increased atmospheric moisture, increased moisture convergence, and a poleward shift in mid-latitude cyclones activity (Christensen et al. 2013; Grise and Polvani 2014). A possible reason of increase precipitation events over southern Ontario in warm season is the poleward movement of tropical cyclones as global warming continues (Jien and Gough 2013; Shawn et al. 2009). However, the detailed

mechanism for the circulation change impacts on the frequency of extreme precipitation events over Ontario is not clear.

This paper focused on four precipitation indices which represent frequency of moderate extremes. The conclusions are based on the data from the relatively worse-case scenario A2 in AR4. Although the trends in annual indices are significant for most ensemble members and are consistent with the recent studies based on AR5 data at global scale (Sillmann et al. 2013), the trends are not significant in seasonal indices in more than half ensemble members. Uncertainties associated with, for example, the representation of observational precipitation with reanalysis precipitation, the relative small ensemble size and the short length of dataset may affect the reliability of the conclusions. The CMIP5 data are currently available; we will use the large GCM ensemble of AR5 data to update the results in the future.

Acknowledgments This research was funded by Ontario Ministry of the Environment and Climate Change.

References

Adamowski K, Bougadis J (2003) Detection of trends in annual extreme rainfal. Hydrol Process 17:3547–3560

Albert MG, Tank K, Zwiers FW*, Zhang X (2009) Guidelines on analysis of extremes in a changing climate in support of informed decisions for adaptation. W WMO—TD No.1500

Baker NC, Huang H-P (2014) A comparative study of precipitation and evaporation between CMIP3 and CMIP5 climate model ensembles in semiarid regions. J Climate 27:3731–3749. doi:10.1175/JCLI-D-13-00398.1

Baldwin D, Desloges J, Band L (2011) Physical geography of Ontario. In: Perera Ajith H, Euler David L, Thompson Ian D (eds) Ecology of a managed terrestrial landscape: patterns and processes of forest landscapes in Ontario. UBC Press, Vancouver

Chiotti Q, Lavender B (2008) In: Lemmen DS, Warren FJ, Lacroix J, Bush E (eds) Ontario; in from impacts to adaptation: Canada in a Changing Climate 2007. Government of Canada, Ottawa, pp 227–274

Christensen JH, Krishna Kumar K, Aldrian E, An S-I, Cavalcanti IFA, de Castro M, Dong W, Goswami P, Hall A, Kanyanga JK, Kitoh A, Kossin J, Lau N-C, Renwick J, Stephenson DB, Xie S-P, Zhou T (2013) Climate phenomena and their relevance for future regional climate change. In: Stocker TF, Qin D, Plattner G-K, Tignor M, Allen SK, Boschung J, Nauels A, Xia Y, Bex V, Midgley PM (eds) Climate Change 2013: the physical science basis. Contribution of Working Group I to the Fifth Assessment Report of the Intergovernmental Panel on Climate Change. Cambridge University Press, Cambridge

Deangelis AM, Broccoli AJ, Decker SG (2013) A comparison of CMIP3 simulations of precipitation over North America with observations: daily statistics and circulation features accompanying extreme events. J. Climate 26:3209–3230. doi:10.1175/JCLI-D-12-00374.1

Dee D, National Center for Atmospheric Research Staff (Eds) (2014) The climate data guide: ERA-Interim. https://climatedataguide.ucar.edu/climate-data/era-interim. Last Modified 03 Nov 2014

Deng Z, Liu J, Zhu H (2015) An evaluation of temperature and precipitation over Ontario in several high resolution reanalysis datasets, 1981–2010 (draft)

Environment Canada, Calculation of the 1981–2010 Climate Normals for Canada. http://climate.weather.gc.ca/climate_normals/normals_documentation_e.html?docID=1981

Gao L, Schulz K, Bernhardt M (2014) Statistical downscaling of ERA-interim forecast precipitation data in complex terrain using LASSO algorithm. Adv Meteorol Article ID 472741

Grise KM, Polvani LM (2014) The response of midlatitude jets to increased CO_2: distinguishing the roles of sea surface temperature and direct radiative forcing. Geophys Res Lett 41:6863–6871. doi:10.1002/2014GL061638

Higgins RW, Kousky VE, Silva VBS, Becker E, Xie P (2010) Intercomparison of daily precipitation statistics over the United States in observations and in NCEP reanalysis products. J Clim 23:4637–4650. doi:10.1175/2010JCLI3638.1

IPCC (2000) IPCC special report emissions scenarios, Summary for policy makers, a special report of IPCC working group III. ISBN: 92-9169-113-5

Jien JY, Gough WA (2013) The influence of Atlantic hurricanes on Southern Ontario's precipitation extremes. Theoret Appl Climatol 114(1–2):55–60

Karl TR, Knight RW (1998) Secular trends of precipitation amount, frequency, and intensity in the United States. Bull Am Meteorol Soc 79(2):231–241

Katz RW (2002) Stochastic modeling of hurricane damage. J Appl Meteorol 41:754–762

Katz RW (2010) Statistics of extremes in climate change. Clim Change 100:71–76

Keim BD, Cruise JF (1998) A technique to measure trends in the frequency of discrete random events. J Clim 11:848–855

Kendall MG (1975) Rank correlation methods. Charless Griffin, London

Kharin V, Zwiers F, Zhang X, Wehner M (2013) Changes in temperature and precipitation extremes in the CMIP5 ensemble. Clim Change 119:345–357. doi:10.1007/s10584-013-0705

Kishore P, Jyothi S, Basha G, Rao SVB, Rajeevan M, Velicogna I, Sutterley TC (2015) Precipitation climatology over India: validation with observations and reanalysis datasets and spatial trends. Clim Dyn 121. doi:10.1007/s00382-015-2597-y

Li G, Zhang X, Zwiers F, Qiuzi H (2012) Quantification of uncertainty in high resolution temperature scenarios for North America. J Clim 25:3373–3388

Maloney ED et al (2014) North American climate in CMIP5 experiments: Part III: Assessment of twenty-first-century projections. J Clim 27:2230–2270. doi:10.1175/JCLI-D-13-00273.1

Mastrandrea MD, Field CB, Stocker TF, Edenhofer O, Ebi KL, Frame DJ, Held H, Kriegler E, Mach KJ, Matschoss PR, Plattner G-K, Yohe GW, Zwiers FW (2010) Guidance note for lead authors of the IPCC fifth assessment report on consistent treatment of uncertainties. Intergovernmental Panel on Climate Change (IPCC). http://www.ipcc.ch

Meehl GA, Covey C, Delworth T, Latif M, McAvaney B, Mitchell JFB, Stouffer RJ, Taylor KE (2007) The WCRP CMIP3 multimodel dataset: a new era in climate change research. Bull Am Meteorol Soc 88:1383–1394

Mladjic B et al (2011) Canadian RCM projected changes to extreme precipitation characteristics over Canada. J Clim 24:2565–2584

Moore BJ, Mahoney KM, Sukovich EM, Cifelli R, Hamill TM (2015) Climatology and environmental characteristics of extreme precipitation events in the Southeastern United States. Mon Wea Rev 143:718–741. doi:10.1175/MWR-D-14-00065.1

National Center for Atmospheric Research Staff (Eds). The Climate Data Guide: NCEP NARR. https://climatedataguide.ucar.edu/climate-data/ncep-narr. Last Modified 20 Nov 2013

Qian B, Zhang X, Chen K, Feng Y, O'Brien T (2010) Observed long-term trends for agroclimatic conditions in Canada. J Appl Meteorol Climatol 49:604–618. doi:10.1175/2009JAMC2275.1

Saha S et al (2010) The NCEP climate forecast system reanalysis. Bull Am Meteorol Soc 91:1015–1057. doi:10.1175/2010BAMS3001.1

Saha S et al (2013) The NCEP Climate Forecast System Version 2. J Clim. doi:10.1175/JCLI-D-12-00823.1

Schmidli J, Frei C, Vidale PL (2006) Downscaling from GCM precipitation: a benchmark for dynamical and statistical downscaling methods. Int J Climatol 26:679–689

Schmith (2007) Statistical and dynamical downscaling of precipitation: an evaluation and comparison of scenarios for the European Alps. J Geophys Res 112:D04105. doi:10.1029/2005JD007026

Sheffield J, Barrett A, Barrie D, Camargo SJ, Chang EKM, Colle B, Fernando DN, Fu R, Geil KL, Hu Q, Jiang X, Johnson N, Karnauskas KB, Kim ST, Kinter J, Kumar S, Langenbrunner B, Lombardo K, Long LN, Maloney E, Mariotti A, Meyerson JE, Mo KC, Neelin JD, Nigam S, Pan Z, Ren T, Ruiz-Barradas A, Seager R, Serra YL, Seth A, Sun D-Z, Thibeault JM, Stroeve JC, Wang C, Xie S-P, Yang Z, Yin L, Yu J-Y, Zhang T, Zhao M (2014) Regional climate processes and projections for North America: CMIP3/CMIP5 differences, attribution and outstanding issues, NOAA Technical Report OAR CPO-2

Shen S, Dzikowski P, Li G, Griffith D (2001) Interpolation of 1961–97 daily temperature and precipitation data onto Alberta polygons of ecodistrict and soil landscapes of Canada. J Appl Meteorol 40:2162–2177

Sillmann J, Kharin VV, Zwiers FW, Zhang X, Bronaugh D (2013) Climate extreme indices in the CMIP5 multi-model ensemble. Part 2: future projections. J Geophys Res. doi:10.1002/jgrd.50188

Solow AR, Moore L (2000) Testing for trend in a partially incomplete hurricane record. J Clim 13:3696–3699

Stefanova L, Misra V, Chan S, Griffin M, O'Brien J, Smith T (2012) A proxy for high-resolution regional reanalysis for the Southeast United States: assessment of precipitation variability in dynamically downscaled reanalysis. Clim Dyn 38:2449–2466

Szeto KK (2008) On the extreme variability and change of cold-season temperatures in Northwest Canada. J Clim 21:94–113. doi:10.1175/2007JCLI1583.1

Thomas R (2009) Changes in the atmospheric circulation as indicator of climate change. In: Letcher TM (ed) Climate change: observed impacts on planet earth. Elsevier, The Netherlands, pp 145–164. ISBN: 978-0-444-53301-2

van Vuuren DP, Edmonds J, Kainuma MLT, Riahi K, Thomson A, Matsui T, Hurtt G, Lamarque J-F, Meinshausen M, Smith S, Grainer C, Rose S, Hibbard KA, Nakicenovic N, Krey V, Kram T (2011) Representative concentration pathways: an overview. Clim Change 109:213–241. doi:10.1007/s10584-011-0148-z

Vincent LA, Mekis E (2006) Changes in daily and extreme temperature and precipitation indices for Canada over the twentieth century. Atmos Ocean 44:177–193

Waggoner PE (1989) Anticipating the frequency distribution of precipitation if climate change alters its mean. Agr Forest Meteorol 47:321–337

Wang XL, Swail VR (2001) Changes of extreme wave heights in northern hemisphere oceans and related atmospheric circulation regimes. J Clim 14:2204–2221

Wang W et al (2011) An assessment of the surface climate in the NCEP climate forecast system reanalysis. Clim Dyn 37:1601–1620

Watterson IG (2005) Simulated changes due to global warming in the variability of precipitation, and their interpretation using a Gamma-distributed stochastic model. Adv Water Resour 28:1368–1381

Widmann ML, Bretherton CS, Salathé EP Jr (2003) Statistical precipitation downscaling over the Northwestern United States using numerically simulated precipitation as a predictor. J Clim 16:799–816

Wigley TML (1988) The effect of changing climate on the frequency of absolute extreme events. Clim Monit 17:44–55 (reprinted in Climatic Change (2009) 97:67–76)

Zhang XB, Vincent LA, Hogg WD, Niitsoo A (2000) Temperature and precipitation trends in Canada during the 20th century. Atmos Ocean 38:395–429

Zhang X, Brown R, Vincent L, Skinner W, Feng Y, Mekis E (2011) Canadian climate trends, 1950–2007. Canadian Biodiversity: Ecosystem Status and Trends 2010, Technical Thematic Report No. 5. Canadian Councils of Resource Ministers. Ottawa, ON

Zwiers FW, Alexander LV, Hegerl GC, Knutson TR, Kossin JP, Naveau P, Nicholls N, Schär C, Seneviratne SI, Zhang X (2013) Climate extremes: Challenges in estimating and understanding recent changes in the frequency and intensity of extreme climate and weather events. In: Asrar GR, Hurrell JW (eds) Climate science for serving society: research, modelling and prediction priorities. Springer, Geneva, pp 339–390